Heterogeneity of murine periosteum osteochondroprogenitors involved in fracture healing

Brya G Matthews[1,2], Francesca V Sbrana[2], Sanja Novak[2], Jessica L. Funnell[2], Ye Cao[1], Emma J. Buckels[1], Danka Grcevic[3], Ivo Kalajzic[2]

[1]Department of Molecular Medicine and Pathology, University of Auckland, Auckland 1142, New Zealand
[2]Department of Reconstructive Sciences, UConn Health, Farmington, CT 06030, USA; UConn Health, Farmington, CT, USA;
[3]Department of Physiology and Immunology, University of Zagreb, Zagreb 10000, Croatia

Supported by: This work has been supported by Connecticut Stem Cell grant 14-SCA-UCHC-02, the Health Research Council of New Zealand Sir Charles Hercus Fellowship, and the American Society for Bone and Mineral Research Rising Star Award to BGM; and NIH/NIAMS grants AR055607 and AR070813 to I.K.

Corresponding author:
Brya G Matthews, Department of Molecular Medicine and Pathology, University of Auckland, Private Bag 92-019, Auckland 1142, New Zealand; brya.matthews@auckland.ac.nz

Abstract

The periosteum is the major source of cells involved in fracture healing. We sought to characterize differences in progenitor cell populations between periosteum and other bone compartments, and identify periosteal cells involved in fracture healing. The periosteum is highly enriched for progenitor cells, including Sca1+ cells, CFU-F and label-retaining cells. Lineage tracing with αSMACreER identifies periosteal cells that contribute to >80% of osteoblasts and ~40% of chondrocytes following fracture. A subset of αSMA+ cells are quiescent long-term injury-responsive progenitors. Ablation of αSMA+ cells impairs fracture callus formation. In addition, committed osteoblast-lineage cells contributed around 10% of osteoblasts, but no chondrocytes in fracture calluses. Most periosteal progenitors, particularly those that form osteoblasts, can be targeted by αSMACreER. We have demonstrated that the periosteum is highly enriched for skeletal stem and progenitor cells and there is heterogeneity in the populations of cells that contribute to mature lineages during periosteal fracture healing.

Keywords: Periosteum, skeletal stem cell, progenitor, alpha smooth muscle actin, osteoblast, fracture

Introduction

Bone tissue retains the ability to heal and regenerate throughout life. This process relies on tissue-resident stem and progenitor cells capable of generating new matrix. Until recently, most studies focused on the bone marrow compartment as a source of osteoprogenitors, with respect to their contribution to growth and remodeling, and their potential as a source of cells for regenerative applications. In the bone marrow compartment, it is well-established that the endosteal region, as well as regions near trabecular bone surfaces, are highly enriched for stem and progenitor cells, including cells of the mesenchymal or skeletal lineage (1, 2). Skeletal stem cells can be isolated from various bone compartments based on their plastic adherence, however, more recently, numerous markers have been proposed to identify or isolate skeletal progenitors prospectively.

The skeleton has different requirements for the functionality of tissue-resident progenitors at different life stages. During development, the majority of the skeleton forms through endochondral ossification via a cartilage template, and this process continues during postnatal life at the growth plates. Hypertrophic chondrocytes can give rise to osteoblasts, particularly those in the primary spongiosa and trabecular region, likely via a progenitor intermediate (3-7). However, this process is growth-related, and skeletal stem cell pools must become established in adult tissues by the completion of growth when the growth plate activity reduces dramatically (as in mice) or fuses completely (in humans). Many stem and progenitor markers have been studied primarily during early life. For example, skeletal progenitors expressing Gli1, Gremlin1, and CTGF are prevalent during development and adolescent growth, but appear to diminish or disappear in mice over one month of age (8-10). Chan and colleagues have reported flow cytometry-based methods for identifying skeletal stem cells (SSC) and downstream bone, cartilage and stromal progenitors (BCSP) as well as various other lineage-restricted populations in mice and humans (11, 12). The murine cell surface antigen combinations were validated in cells isolated from whole neonatal mouse long bones, but have since been applied to various settings in adult systems including fracture healing without further validation (13, 14). Similarly, markers for putative SSCs in humans were identified using fetal tissue, with a focus on the hypertrophic cartilage zone, then applied to adult tissue. Another recent study used similar marker combinations to identify stem cell populations in the periosteum, with the majority of studies performed using very young animals (late embryonic up to P32, many at P6) (15). PDGFRα+Sca1+ (PαS) cells were characterized in adult animals, and Leptin receptor Cre-labeled cells that ultimately give rise to osteoblasts and bone marrow adipocytes do not become established before two months of age (2, 16). These results indicate that stem and progenitor cell populations and markers change at

different life stages, meaning that markers identified in neonates or juveniles should not be applied to the adult setting without additional validation.

The periosteum is the tissue surrounding the outer surface of the bone. It is physically separated from the bone marrow compartment, and appears to have a much greater regenerative capacity, playing a critical role in fracture healing (17, 18). Periosteum-based healing involves a process similar to endochondral ossification. Following an inflammatory phase, the periosteum expands and forms a callus initially comprised of fibrocartilage in the central area, combined with direct bone formation at the periphery. It has been challenging to identify markers that are specific to the periosteum, however recent studies have characterized cathepsin K and periostin as markers that are highly enriched in periosteal mesenchymal cells, and alpha smooth muscle actin (αSMA) was shown to enrich Mx1-labeled periosteal cells for progenitors (15, 19, 20). We have previously shown that αSMA identifies a population of growth-related osteoprogenitors in the trabecular region, and cells that contribute to fracture healing in the adult periosteum (21, 22).

In the current study, we have evaluated the expression of stem/progenitor markers in different bone compartments, and evaluated growth potential of different periosteal populations ex vivo. We have also characterized contribution to fracture callus formation by various populations of cells within the periosteum, showing that αSMA identifies a subset of long-term progenitors.

Results

Putative mesenchymal stem cell markers are enriched in periosteum

There are numerous markers for skeletal stem and progenitor cells that have been reported in the literature, however many have not been evaluated systematically in different tissue compartments. We evaluated the expression of several cell surface markers in periosteum, endosteum and bone marrow of adult mice (Fig. 1A, Fig. S1). All stains included a CD45/CD31/Ter119 cocktail to exclude hematopoietic and endothelial cells and select for mesenchymal lineages (termed CD45- population). We confirmed that the freshly isolated CD45+ population was unable to form CFU-F. The CD45- cells in periosteum were highly enriched for most of the markers evaluated compared to both endosteum and bone marrow (Fig. 1A). Sca1, PDGFRα and PDGFRβ were abundant in periosteum, but expressed on <2% CD45- endosteal and bone marrow cells. The only marker that did not follow this trend was CD105, which was consistently present on the majority of endosteal CD45- cells. Various marker combinations that have previously been used to identify stem cells such as Sca1/PDGFRα or Sca1/CD51 were easily identifiable in periosteum but very rare in the endosteum or bone marrow (Fig. S1). The CD45- periosteal population formed around 20x more CFU-F than endosteum, suggesting functional enrichment for stem and progenitor cells (Fig. 1B). Stem/progenitor markers or combinations should, by definition, exclude mature cell types of the lineage. There are not any well-established methodologies to identify osteoblasts using cell surface markers, although some authors report Sca1+CD51+ as stem cells and Sca1-CD51+ cells as committed osteoprogenitors or osteoblasts (23, 24). We utilized the Col2.3GFP transgene to identify mature osteoblasts (25). Col2.3GFP+ cells were always present in endosteal samples (6.7±5.1% of CD45-) and were detectable in numbers sufficient for analysis in some periosteum samples (1.0±1.1% of CD45-). We found that around 30% of endosteal osteoblasts were CD51+ (Fig. 1C) (26). A subset of osteoblasts in both tissues were CD105+, while the other markers were rare or absent in endosteal osteoblasts. We also evaluated the utility of the stain described by Chan et al. to identify SSC and BCSP (12). The gating strategy is shown in Fig. 1D. We found that Col2.3GFP+ osteoblasts constituted around a third of cells defined as both SSC (CD45-CD51+CD90-6C3-CD105-) and BCSP (CD45-CD51+CD90-6C3-CD105+) in endosteal preparations (Fig. 1D). In addition, when we evaluate the proportion of SSC and BCSP in different tissue compartments, we find that GFP+ osteoblasts have the highest frequency of these 'stem cells' (Fig. 1E). Therefore, these marker combinations used for SSC and BCSP do not exclude mature cells within the lineage in adult mice, so do not specifically identify stem cells in this setting.

We went on to evaluate the expansion and differentiation potential of selected periosteal populations using in vitro assays. CFU-F formation was restricted to CD51+ cells, and most enriched in Sca1+ CD51+

cells (Fig. 1F). CD90+ cells also showed high CFU-F potential, whereas CD105+ cells, which are almost exclusively CD90-, formed few or no colonies. Sca1+ CD51+ cells showed the ability to differentiate towards osteogenic (ALP+) and adipogenic (Oil Red O+) lineages, in many cases within a single colony (Fig. 1G). Similar results were obtained for the CD90+ population. Sca1- CD51+ cells and CD90- CD105- cells efficiently activated ALP, but never differentiated into adipocytes, suggesting that in addition to including some mature osteoblasts, these populations contain committed osteoprogenitors that remain capable of density-independent growth.

Label-retaining cells in the periosteum are enriched for progenitor markers

One feature of long-term stem cells is a slow cycling rate, and this can be evaluated experimentally using label retention assays. We used a dox-inducible GFP-tagged histone system, H2B-GFP, which is incorporated into the DNA during dox feeding, then diluted during subsequent cell division. This system has been used to enrich for highly self-renewing populations of hematopoietic stem cells and muscle satellite cells (27, 28). The experimental design for generating LRCs is shown in Fig. 2A. We were able to incorporate H2B-GFP into the majority of periosteal cells (Fig. 2B, Fig. S2). Quiescent terminally differentiated cells such as osteocytes also effectively retain the label (Fig. 2C). Flow cytometry was used to track GFP expression in the CD45- fraction of the periosteum (Fig. 2D-E). After the chase phase, the periosteum contained a small population of true LRCs (GFP^{hi}), as well as a slightly larger GFP^{int} population which would be expected to contain some LRCs. Histologically, these cells were mostly in the inner cambium layer of the periosteum. We confirmed that most cells capable of forming CFU-F initially received a GFP label (Fig. 2F). After the chase, both GFP+ populations showed enrichment of CFU-F compared to the GFP- fraction (Fig. 2G). We also evaluated cell surface marker expression in LRCs, and found strong enrichment of Sca1 and CD51, more frequent expression of CD90, and fewer CD105+ cells in periosteum (Fig. 2H) and endosteum (Fig. 2I) compared to GFP- cells.

In vivo identification of long-term osteochondroprogenitors

We have previously demonstrated that αSMACreER identifies osteoprogenitors in both periosteum and the bone marrow compartment (21, 22, 29). Previously, we delivered tamoxifen at the time of fracture, which potentially labels cells that activate αSMA expression at the time of or shortly after fracture (30). In this study, we delivered tamoxifen up to 90 days before fracture to evaluate whether the reporter was identifying long-term progenitor cells. Firstly, we confirmed that αSMA-labeled cells were retained in the periosteum over the experimental time course by both histology (Fig. 3A-B) and flow cytometry (Fig. 3C). αSMA-labeled cells remained in the periosteum at a similar frequency over the timeframe evaluated, and also remained in the endosteum (Fig. 3D). In juvenile mice (4-5 weeks

old), we see contribution of αSMA+ cells from the bone marrow, particularly in the trabecular region, to osteoblasts and osteocytes after 17 days (Fig. S3A-B) (22). However, 70 days after tamoxifen delivery, osteoblasts are no longer labeled, but some Tomato+ osteocytes remain (Fig. S3C). In contrast, when tamoxifen is delivered to sexually mature mice, there is no contribution to osteoblasts in trabecular bone up to 100 days after tamoxifen (Fig. S4).

Following tibial fracture, αSMA-labeled cells in the periosteum made substantial contributions to fracture callus osteoblasts and chondrocytes (Fig. 3E-F, H-J). Very few Tomato+ cells contributed to mature cell types in the absence of tamoxifen (Fig. 3H-J, Fig. S5A). Most fracture callus osteoblasts are derived from cells that expressed αSMA at some point in their lineage, with 81.5% derived from αSMA+ cells labeled just after fracture. A smaller population of osteoblasts were derived from long-term αSMA-labeled progenitors (around 20%, Figure 3H-I). Contribution to chondrocytes showed a very similar trend based on the timing of tamoxifen, however the proportion of Tomato+ chondrocytes was always lower (Figure 3J). Following the fracture, bone formation also occurs inside the marrow compartment, particularly in the proximal diaphysis surrounding the pin (Fig. S5). αSMA-labeled cells labeled at the time of fracture make a major contribution to newly formed osteoblasts in the marrow compartment, however, there was less contribution at the later time points suggesting that αSMA identifies long-term injury-responsive osteochondroprogenitors in the periosteum, but does not consistently label long-term injury-responsive cells in the bone marrow compartment.

We also tested the hypothesis that mature osteoblast lineage cells may contribute to osteoblast formation in the fracture callus. Col2.3CreER-labeled cells made a small but significant contribution to osteoblast formation in the fracture callus, but only when tamoxifen was given close to the time of fracture (Fig. 3G, K). We did not detect any contribution of Col2.3-labeled cells to chondrocytes.

<u>αSMA identifies transplantable osteoprogenitors</u>

We next performed further characterization of αSMA-labeled cells in the absence of injury. By flow cytometry, we confirmed that αSMA+ cells were much more prevalent in periosteum of adult mice compared to endosteum and bone marrow (Fig. 4A-B). We evaluated expression of various markers in the αSMA+ population. The majority of αSMA-labeled cells in the periosteum and endosteum express CD51 and CD90 (Fig. 4C-D). The other markers tested were expressed in smaller subsets of αSMA-labeled cells, indicating there is heterogeneity within the labeled population. We next evaluated whether the prevalence of any of these markers in the αSMA-labeled population changed over time since labeling. We did not detect differences in the level of expression of any of the markers

evaluated individually or in various combinations at different times after tamoxifen, suggesting that additional markers may be required to define the heterogeneity and phenotype of these cells (Fig. 4E).

In *ex vivo* assays, αSMA+ periosteal cells were capable of CFU-F formation (Fig. 4F). Following transplantation into a critical-sized calvarial defect, αSMA+ cells were readily identified in all sections evaluated, indicating the ability to engraft and expand in the defect (Fig. 4G). Some cells activated Col2.3GFP indicating some differentiation into osteoblasts, similar to a recent study (20). We also investigated whether αSMA-labeled cells contained LRCs (Fig. 4H). Initially, we labeled 73.4±7.6% of αSMA+ cells, and after at least 13 weeks chase, 22.6±7.7% were LRCs, indicating a large proportion of these cells are quiescent. This is a substantially higher proportion of LRCs than we found in the overall CD45- population of the same samples (3.2±1.5%, $p<0.0001$). *Ex vivo*, αSMA-labeled LRCs (GFP+Tom+) were enriched for CFU-F compared to the GFP-Tom+ population (Fig. 4I). Interestingly, αSMA-labeled LRCs appeared to be lineage-restricted, with evidence of differentiation along the osteogenic lineage, but absence of adipogenic differentiation (Fig. 4J). αSMA-labeled LRCs were more frequently CD51+, but fewer were CD90+ that Tomato+ non-LRCs (Fig. 4K).

Functional contribution of αSMA+ cells to fracture healing

We evaluated the functional importance of αSMA+ cells to fracture healing using the Rosa-DTA model of cellular ablation. When ablation was performed at the time of fracture (day 0, 1) we saw a 50% reduction in αSMA-labeled cells in 4 DPF callus tissue by flow cytometry (Fig. 5A) and a clear reduction in fracture size and αSMA-labeled cells by histology (Fig. 5B). At 14 DPF there was a significant reduction in total callus volume as well as callus bone mass (Fig. 5C-D). Similar impairments in healing were seen whether ablation was performed at the time of fracture, or throughout the first 8 days of healing, suggesting that early loss of αSMA+ cells was most important for this phenotype.

Discussion

We confirmed that the periosteum is highly enriched for cells with markers and phenotype of stem and progenitor cells. There is abundant evidence suggesting that fracture healing is impaired if periosteum is removed, or that otherwise critical-sized defects in a variety of bones can regrow if periosteum is retained (31-34). There are also numerous studies reporting superior outcomes with cultured periosteal cells compared to other cell sources like bone marrow in terms of bone formation both in vitro and in vivo (19, 35). Of the markers we examined, we found that most were much more abundant in the periosteum than endosteum. Sca1, CD51, CD90 and PDGFRα (36) all enrich for CFU-F in periosteum, similar to what has been reported in other cell types. Although we did not thoroughly characterize PαS cells in the periosteum, we note that these cells were very rare in the endosteal compartment. Morikawa et al. report large enrichment of PαS cells following collagenase digestion of crushed bones (2). Our results raise the possibility that the cells isolated in their studies were actually derived from the periosteum. With respect to CD51, our results agree with the studies using neonatal bones indicating that progenitor cells are solely contained within the CD51+ population (37), however, a significant proportion of mature osteoblasts are CD51+, so additional markers that exclude differentiated cells are required.

CD105 may not be a useful marker of mesenchymal stem and progenitor cells during adulthood *in vivo*. In addition to being the only marker that was more prevalent in endosteum than periosteum, CD105 was also mostly absent from LRCs in all cell types analyzed. CD105+ periosteal cells also failed to form CFU-F. CD105 is best known as one of the markers used to identify 'MSCs' in culture, but has also been used as part of stains to identify or enrich for progenitor populations in the periosteum and other tissues (12, 15, 16, 20). We demonstrated that the BCSP and SSC marker combinations, which were originally developed using neonatal bones, contain a significant proportion of mature osteoblasts in adult bones. This likely influences the observation that these populations expand in settings such as BMP2 treatment or fracture healing, which means some results should be revisited in future when more specific markers for adult bone-residing progenitors are developed (12, 13). Interestingly, a similar stain with the addition of CD200 was used to enrich for periosteal stem cells in a recent study (15).

Label-retaining cells in the periosteum showed large differences in cell surface marker profile to non-LRCs, and enrichment for CFU-F formation. However, the experimental system presented some limitations, as we did not achieve uniform labeling initially, and some cells had low GFP expression even in the absence of dox. This may be related to positioning of the tetO-H2B-GFP cassette in the

Col1a1 locus. The use of label retention is likely to perform better in combination with other markers that already enrich for stem cell populations (27, 28). Within the αSMA-labeled population, we saw 4-fold higher CFU-F frequency than αSMA-labeled non-LRC cells. A previous study also reported the presence of heterogeneous LRCs in the periosteum, however they were unable to perform functional characterisation (38). Interestingly, they report the absence of αSMA+ LRCs, however many antibodies to αSMA stain perivascular cells in larger blood vessels, but do not detect αSMA+ cells in the cambium layer of the periosteum. The αSMA+ cells in the cambium layer appear to be the cell subset involved in fracture healing (20, 39). Label-retention may be a useful tool to enrich for periosteal stem cells in ex vivo assays, although more robust assays for testing self-renewal such as serial transplantation are required.

One of the key findings of this study is that αSMA identifies long-term, slow-cycling osteoprogenitors in the adult periosteum that are functionally important for bone and cartilage formation during fracture healing. αSMA+ periosteal cells also contribute to osteoblasts in response to loading (29). The lineage tracing results suggest that αSMA identifies at least two distinct osteochondroprogenitor populations in the periosteum that contribute to fracture healing. Firstly, there is a long-term quiescent tissue-resident progenitor population that contributes to a subset of osteoblasts and chondrocytes for at least 3 months after labeling. Secondly, there are cells that activate αSMA after injury, as visualized in studies using real-time αSMA reporters (30). The majority of osteoblasts are derived from αSMA-labeled cells when tamoxifen is given at the time of fracture. The results from the fractures performed after a two-week chase, which show slightly lower contribution than at the time of fracture, but a trend towards higher contribution than after six or more weeks chase suggest that there may be a third population of tissue-resident osteochondroprogenitor cells that have a limited lifespan or lack self-renewal capacity. We were unable to see any time-dependent shifts in the cell-surface markers analyzed in order to dissect these different populations.

We consistently saw lower contribution of αSMA to chondrocytes than to osteoblasts. This may be due to contribution of muscle-derived cells to chondrocytes (40, 41). Notably, αSMA expression is present in some muscle cells, both myogenic satellite cells, and a separate population of stromal cells that can contribute to heterotopic bone formation (42, 43). It is also possible that there is a periosteal population that is restricted to chondrogenic and perhaps fibroblastic lineages, although we are not aware of any cell populations that have shown these properties *in vivo*. Gli1+ cells contributed to more chondrocytes than osteoblasts in a similar fracture model (8). Gli1+ cells also formed fibrous tissue in fractures that failed to heal due to radiation exposure, while αSMA+ cells did not (39). The contribution

of Gli1+ cells in the fibrous layer of the periosteum, or from non-periosteal sources could explain these observations. Cxcl12-CreER also appears to identify cells that form mainly chondrocytes in a periosteal fracture callus, however the presence of labeled cells outside the bone marrow compartment was not evaluated making it difficult to identify the tissue where these cells originated (44).

Lineage tracing with Col2.3CreER indicated that there are cells the periosteum already committed to the osteogenic lineage that participate in osteoblast expansion during fracture healing. Cells labeled by Prx1, Col2, Cathepsin K, LepR and Mx1-driven Cres all make a major contribution to fracture callus osteoblasts, however all these models involve either constitutive Cre expression, or long-term labeling that includes differentiated cells, meaning that a combination of stem/progenitor cells and pre-osteoblasts/osteoblasts could be contributing to new osteoblast formation (15, 16, 19, 20, 39). Prx1-CreER and Sox9-CreER also label cells in the periosteum that contribute to fracture healing (45, 46). It is unclear if these populations overlap with αSMA+ cells or represent separate progenitor pools. However, our results suggest that there is heterogeneity in the cell types contributing to both osteoblasts and chondrocytes in the fracture callus, but by administering tamoxifen at the time of fracture, the majority of periosteal progenitors, particularly those that form osteoblasts, can be targeted by αSMACreER.

αSMA+ cells are present in the endosteum, but are less frequent than in the periosteum. αSMA is expressed in a growth-related transiently amplifying progenitor population in the trabecular region. It is also activated in cells in situations where there is a greater need for osteoblasts, such as injury, or genetic ablation of osteoblasts (26, 47). However, it does not appear to label cells involved in bone turnover during adulthood, or consistently label long-term injury responsive cells in the bone marrow compartment. αSMA also labels cells involved transiently in tendon growth, as well as identifying progenitors of cementoblasts and periodontal fibroblasts in the periodontium (48, 49). αSMA+ cells are also a major contributor to healing in both these tissues, as well as during reparative dentinogenesis following injury in murine molars (50). There is increasing evidence in bone tissue that different cell types could contribute to homeostasis compared to regeneration. In calvarial bones, the suture provides a niche for cells involved in both growth and healing. Axin2+ and Gli1+ cells contribute to both growth and healing, however Prx1CreER labels a more restricted population only involved in healing (51-53). Cxcl12+ cells in the central bone marrow do not contribute osteoblast formation under homeostatic conditions, but are activated and recruiting following injury involving the bone marrow (44). αSMA+ cells in the periosteum appear to represent a population involved primarily in response to injury, or increased need for bone formation.

In conclusion, we have demonstrated that the periosteum is highly enriched for mesenchymal stem and progenitor cells compared to endosteum and bone marrow. We have also identified different populations of cells with regenerative potential within the periosteum. Our data demonstrate the presence of a long-term periosteum residing osteochondroprogenitor cell that is identified by expression of αSMA, along with injury-activated αSMA+ progenitors and mature Col2.3+ osteoblasts that also contribute to the healing process.

Methods

Mice

All animal studies were approved by the institutional animal care and use committee at UConn Health or the University of Auckland. αSMACreER and Col2.3GFP mice have been described (22, 25). R26-M2rtTA; TetOP-H2B-GFP dual homozygous mice were purchased from Jackson Labs (stock # 016836) (27), as were Ai9 Tomato reporter mice (007909, (54)), Rosa-DTA (009669, (55)) and Col2.3CreER (016241, (56)). All these strains were maintained on a C57Bl/6J background. NSG immunodeficient mice (NOD.Cg-Prkdcscid Il2rgtm1Wjl/SzJ, stock # 005557) were a gift from David Rowe. All transgenic mice for experiments were bred at UConn Health and were group housed in individually ventilated cages maintained at 22 ± 2°C, 55 ± 5% humidity and a 12h light-dark cycle and allowed ad libitum access to food and water. Male C57Bl/6J mice were used for experiments at the University of Auckland and were bred at the onsite facility under similar conditions. CreER was activated by tamoxifen in corn oil (75µg/g ip), unless otherwise stated, two doses of tamoxifen were administered 24h apart. Animals were assigned to experimental groups in blocks, and cage-mates were generally exposed to the same tamoxifen regimen to avoid inadvertent exposure of low-dose tamoxifen.

Cell isolation

For studies comparing different tissue compartments, bone marrow, endosteum and periosteum were isolated from hindlimbs of the same mice as previously described (26, 36). In most cases, 2-3 animals of the same sex were pooled to generate a sample. Briefly, after removal of muscle tissue, bone marrow was flushed and underwent red blood cell lysis (57). Periosteum was scraped off the bone surface and digested in PBS containing 0.05% Collagenase P (Roche, IN, USA) and 0.2% hyaluronidase (Sigma Aldrich, St Louis, MO, USA) for 1h at 37°C. To isolate endosteal cells, bones were then opened, crushed, loosely attached cells removed by washing, then digested in PBS containing 0.05% Collagenase P for 1h at 37°C. Cells were washed and resuspended in staining medium (SM, 2% FBS, 1mM EDTA in PBS).

Flow cytometry and cell sorting

Cells were stained using antibody cocktails in SM. Antibodies and secondary reagents are listed in Table 1. Analysis was performed on an LSRII or Aria II instrument (BD Biosciences), and sorting was performed on an Aria II. All experiments included unstained controls for establishing gates derived from non-fluorescent mice, and single color controls generated using periosteal or bone marrow cells. Some experiments included FMO controls to assist with gating. Dead cells were excluded in most experiments using DAPI staining (~50ng/ml final concentration). Four-way sorting was performed on

selected populations. Cells were sorted into 1.5ml tubes containing 500µl collection medium (αMEM 10% FBS). Acquisition and sorting was performed using FACSDiva software and analysis was performed in FlowJo (BD Biosciences). Experiments generally involved at least 2 biological replicates per group, and most were performed on more than one occasion to ensure consistent outcomes.

In vitro assays

Colony forming unit fibroblast (CFU-F) assays were performed using freshly sorted cells. Live cell numbers were assumed to be 50% of the cells sorted by the machine. Sorted cells were resuspended in αMEM 20% FBS and seeded in 6-well plates, generally at 50 cells/cm^2, although this varied depending on yield. In most cases, 3 wells were seeded per population, and at least 3 independent samples per population were evaluated. Cells were cultured in a 37°C humidified incubator, 5% O_2, 5% CO_2. Medium was changed on day 4, and cultures were terminated for staining on day 7-8. Cells were fixed in 10% formalin for 10 min, washed in water, then underwent crystal violet staining. For differentiation, after 7 days, medium was changed to an osteogenic/adipogenic combined cocktail containing αMEM 10% FBS 50µg/ml ascorbic acid, 4mM β-glycerophosphate, 1µM insulin, 0.5µM rosiglitazone, and transferred to a normoxic incubator. Medium was changed after 3 days and cultures were terminated after 5 days and underwent ALP staining (86R or B5655, Sigma Aldrich) and Oil Red O staining, followed by imaging then crystal violet staining.

Label retention studies

R26-M2rtTA; TetOP-H2B-GFP (H2B-GFP) males were crossed with αSMACreER/Ai9/Ai9 females to generate experimental mice. Mice received doxycycline (dox) in their diet (625mg/kg, Teklad Custom Diet TD.01306, Envigo, Madison, WI) from P10 for 5 weeks. Males were removed from breeding cages prior to birth of pups to ensure mothers did not ingest dox during subsequent pregnancies. Some animals received two doses of ip tamoxifen at the time of dox withdrawal. The chase period was a minimum of 13 weeks. Animals that were never exposed to dox were included in all experiments as controls.

Tibia fracture

Closed tibia fractures stabilized by an intramedullary pin were generated mid-shaft as previously described (21). All mice undergoing fracture lineage tracing were female, and were sexually mature young adults (8-16 weeks of age at tamoxifen administration, 8-24 weeks at fracture). The presence of fracture was confirmed by X-ray (Faxitron LX 60). Animals were euthanized and limbs collected for histology 7 or 14 days post fracture (DPF).

Histology

Bones were fixed for 5-7 days in 4% paraformaldehyde, incubated in 30% sucrose overnight and embedded in cryomatrix (Fisher Scientific). Cryosections (7µm) were obtained using a cryostat and tape transfer system (Section-lab, Hiroshima, Japan) as previously described (58). Imaging settings were kept consistent for each dataset. Fluorescent images were obtained with an Axioscan slide scanner (Zeiss). Immunostaining antibodies are listed in Table 1. For Sox9 staining, sections were permeabilized in 0.1% Triton X for 15 min, blocked in 2% BSA/PBS for 1h, and stained with Sox9 antibody overnight at 4°C. For osterix staining, sections were permeabilized in 0.1% Tween-20 for 15 min, blocked in 10% goat serum, 2% BSA/PBS for 1h, stained with anti-Osterix antibody overnight at 4°C. Both sets of slides were washed in 0.1% Tween-20/PBS and stained with secondary antibody for 1h at RT then washed thoroughly. Slides were coverslipped in glycerol/PBS containing DAPI. Image analysis was performed as described previously using ImageJ (29). Samples were excluded from all image analysis for the following reasons: fracture was not evident or callus was absent. For osteoblast analysis, sections were excluded if they did not contain a clear fracture site. Endosteal analysis was only performed in sections that had a clear central marrow cavity present, and new bone formation evident in this region. Chondrocyte analysis was performed at day 7 only, as most cartilage is gone by day 14, and some fractures were excluded due to lack of cartilage tissue for analysis. Briefly, to evaluate Tomato+ contribution to osteoblasts, ROIs were drawn encompassing the fracture callus. Adjacent ROIs encompassing the central area of the callus (1mm either side of the fracture site) as well as more distal regions were drawn (up to 6 ROIs/section), then data were pooled to determine total callus values. The DAPI channel was thresholded and separated using the watershed algorithm, then fluorescent signal for each channel was measured in nuclear regions. Standardized thresholds were set manually for each channel. We could then calculate the proportion of cells that were GFP+ or Osx+ (osteoblasts), the proportion that were Tomato+, and the fraction of osteoblasts that were Tomato+. In most cases, 1 section/bone was analyzed. Where multiple sections were analyzed, results from different sections were consistently very similar and were pooled. A minimum of 3000 nuclei (median 9262) were evaluated for each sample. Similar analysis was performed on the bone marrow compartment when sections were suitable. For chondrocyte analysis, since there was some non-specific staining with the Sox9 antibody, only regions that demonstrated chondrocytic morphology were incorporated in the analysis ROIs.

Calvarial defect transplantation

Briefly, mice were anesthetized with ketamine/xylazine (135 mg/kg and 15 mg/kg) and bilateral critical-sized circular defects (3.5 mm diameter) created in the parietal bone. 2500-5000 sorted αSMA-labeled cells were mixed with $2x10^5$ BMSCs, resuspended in 7 ul PBS, loaded on a healos scaffold and placed into calvaria defects of immunodeficient NSG mice (n=6). After five weeks, mice were euthanized for histological analysis.

Ablation studies

Animals were generated by crossing Rosa-DTA homozygous mice with SMACreER, or where lineage tracing was required, crossing SMACreER/Rosa-DTA with Ai9 and using only Cre+ animals. Fractures were performed in 7-10-week-old animals as previously described (59). Tamoxifen was given 0 and 1 DPF in most cases. Briefly, closed transverse diaphyseal femoral fractures were created using a blunt guillotine, after inserting a 24G needle into the intramedullary canal. Fractures were confirmed immediately after the procedure and the healing process was monitored by X-ray (Faxitron LX 60). To evaluate efficacy of the ablation, flow cytometry and histology were performed 4 DPF. For flow, the callus tissue was dissected and single cell suspension from individual male mice (n=4) was generated, stained with CD45/CD31/Ter119 cocktail and DAPI. For microCT, fractured bones were collected 14 DPF, fixed in 10% formalin, and scanned (µCT40, Scanco Medical AG, Bassersdorf, Switzerland) with a voxel size of 12 µm, 55 kV and intensity of 145 µA. We evaluated 150 slices above and below the fracture site to measure density, and callus volume and calculate bone mass. An additional group given tamoxifen 0, 2, 4, 6 and 8 DPF were included. Controls with different tamoxifen regimens showed no difference between groups so were pooled. Both male and female mice were included (Cre- n=14, 8M 6F; DTA D0,1 n=10, 4M 6F; DTA D0-8 n=8 4M 4F).

Statistics

All experiments include at least three biological replicates. For lineage tracing fracture experiments, we planned to include at least n=6 per group, although long-term tracing groups in particular had more animals included to account for possible exclusions. We planned to include n=10 for DTA studies based on our previous experience with quantitative fracture studies, but numbers and sex distribution were limited by the genotypes of available animals. Exact n values are listed in figures or figure legends, or where ranges are stated, in the source data files. Values represent the number of biological replicates (biological replicates represent 1 mouse/1 fracture for injury studies, and one pool of 2-3 mice for most flow cytometry studies; most of the flow and CFU-F data involves analysis or sorts performed over multiple days or experiments). Graphs show mean ± standard error of the mean. Statistical analysis was performed in Graphpad Prism, using t-tests or one-way or two-way ANOVAs

with appropriate post-hoc tests. For many of the flow cytometry datasets where different populations or tissues from one sample are evaluated, paired tests are used. Details are included in figure legends, and analysis or p values are supplied in the source data files. $P<0.05$ was used as the threshold for statistical significance.

Acknowledgements

This work has been supported by Connecticut Stem Cell grant 14-SCA-UCHC-02, the Health Research Council of New Zealand Sir Charles Hercus Fellowship, and the American Society for Bone and Mineral Research Rising Star Award to BGM; and NIH/NIAMS grants AR055607 and AR070813 to I.K. We thank Prof. David Rowe for providing NSG mice. We thank Drs Emilie Roeder and India Azevedo for assistance with fracture studies, and Dr Liping Wang for performing some of the calvarial defect surgeries.

Table 1: Antibodies and related reagents used in this study

Antibodies used for flow cytometry					
Antigen	Conjugate	Manufacturer	Clone	Cat #	Dilution
CD45	eFluor450	eBioscience	30-F11	48-0451	1:400
Ter119	eFluor450	eBioscience	TER-119	48-5921	1:200
CD31	eFluor450	eBioscience	390	48-0311	1:400
CD45	APC	eBioscience	30-F11	17-0451	1:400
Ter119	APC	eBioscience	TER-119	17-5921	1:200
CD31	APC	eBioscience	390	17-0311	1:400
CD140a	APC	eBioscience	APA5	17-1401	1:100
CD140a	PE-Cy7	eBioscience	APA5	25-1401	1:400
CD140b	APC	eBioscience	APB5	17-1402	1:100
CD105	APC	eBioscience	MJ7/18	17-1051	1:200
CD90.2	APC eFluor 780	eBioscience	53-2.1	47-0902	1:200
CD90.2	BV605	BD Bioscience	30-H12	740334	1:100
CD51	Biotin	eBioscience	RMV-7	13-0512	1:100
Sca1	AlexaFluor700	eBioscience	D7	56-5981	1:100
Ly51	BV711	BD Bioscience	6C3	740691	1:100
Immunostaining antibodies					
Sox9		EMD Millipore		ABE2868	1:200
Osterix		Abcam		ab209484	1:400
Secondary reagents					
Streptavidin APC eFluor 780		eBioscience		47-4317	1:400
Streptavidin PE-Cy7		eBioscience		25-4317	1:400
Streptavidin APC		eBioscience		17-4317	1:400
Goat anti rabbit AlexaFluor647		ThermoFisher		A21244	1:300

References:

1. Siclari VA, Zhu J, Akiyama K, Liu F, Zhang X, Chandra A, et al. Mesenchymal progenitors residing close to the bone surface are functionally distinct from those in the central bone marrow. Bone. 2013;53(2):575-86.
2. Morikawa S, Mabuchi Y, Kubota Y, Nagai Y, Niibe K, Hiratsu E, et al. Prospective identification, isolation, and systemic transplantation of multipotent mesenchymal stem cells in murine bone marrow. J Exp Med. 2009;206(11):2483-96.
3. Wolff LI, Hartmann C. A second career for chondrocytes—transformation into osteoblasts. Curr Osteoporos Rep. 2019;17(3):129-37.
4. Yang L, Tsang KY, Tang HC, Chan D, Cheah KS. Hypertrophic chondrocytes can become osteoblasts and osteocytes in endochondral bone formation. Proc Natl Acad Sci U S A. 2014;111(33):12097-102.
5. Yang G, Zhu L, Hou N, Lan Y, Wu XM, Zhou B, et al. Osteogenic fate of hypertrophic chondrocytes. Cell Res. 2014;24(10):1266-9.
6. Zhou X, von der Mark K, Henry S, Norton W, Adams H, de Crombrugghe B. Chondrocytes transdifferentiate into osteoblasts in endochondral bone during development, postnatal growth and fracture healing in mice. PLoS Genet. 2014;10(12):e1004820.
7. Mizuhashi K, Ono W, Matsushita Y, Sakagami N, Takahashi A, Saunders TL, et al. Resting zone of the growth plate houses a unique class of skeletal stem cells. Nature. 2018;563(7730):254-8.
8. Shi Y, He G, Lee WC, McKenzie JA, Silva MJ, Long F. Gli1 identifies osteogenic progenitors for bone formation and fracture repair. Nat Commun. 2017;8(1):2043.
9. Worthley DL, Churchill M, Compton JT, Tailor Y, Rao M, Si Y, et al. Gremlin 1 identifies a skeletal stem cell with bone, cartilage, and reticular stromal potential. Cell. 2015;160(1-2):269-84.
10. Wang W, Strecker S, Liu Y, Wang L, Assanah F, Smith S, et al. Connective Tissue Growth Factor reporter mice label a subpopulation of mesenchymal progenitor cells that reside in the trabecular bone region. Bone. 2015;71:76-88.
11. Chan CKF, Gulati GS, Sinha R, Tompkins JV, Lopez M, Carter AC, et al. Identification of the human skeletal stem cell. Cell. 2018;175(1):43-56 e21.
12. Chan Charles KF, Seo Eun Y, Chen James Y, Lo D, McArdle A, Sinha R, et al. Identification and specification of the mouse skeletal stem cell. Cell. 2015;160(1–2):285-98.
13. Marecic O, Tevlin R, McArdle A, Seo EY, Wearda T, Duldulao C, et al. Identification and characterization of an injury-induced skeletal progenitor. Proc Natl Acad Sci U S A. 2015;112(32):9920-5.
14. Tevlin R, Seo EY, Marecic O, McArdle A, Tong XM, Zimdahl B, et al. Pharmacological rescue of diabetic skeletal stem cell niches. Sci Transl Med. 2017;9(372).
15. Debnath S, Yallowitz AR, McCormick J, Lalani S, Zhang T, Xu R, et al. Discovery of a periosteal stem cell mediating intramembranous bone formation. Nature. 2018;562(7725):133-9.
16. Zhou BO, Yue R, Murphy MM, Peyer JG, Morrison SJ. Leptin-receptor-expressing mesenchymal stromal cells represent the main source of bone formed by adult bone marrow. Cell Stem Cell. 2014;15(2):154-68.
17. Colnot C. Skeletal cell fate decisions within periosteum and bone marrow during bone regeneration. J Bone Miner Res. 2009;24(2):274-82.
18. Roberts SJ, van Gastel N, Carmeliet G, Luyten FP. Uncovering the periosteum for skeletal regeneration: The stem cell that lies beneath. Bone. 2015;70:10-8.
19. Duchamp de Lageneste O, Julien A, Abou-Khalil R, Frangi G, Carvalho C, Cagnard N, et al. Periosteum contains skeletal stem cells with high bone regenerative potential controlled by Periostin. Nat Commun. 2018;9(1):773.
20. Ortinau LC, Wang H, Lei K, Deveza L, Jeong Y, Hara Y, et al. Identification of functionally distinct Mx1+alphaSMA+ periosteal skeletal stem cells. Cell Stem Cell. 2019;25(6):784-96.

21. Matthews BG, Grcevic D, Wang L, Hagiwara Y, Roguljic H, Joshi P, et al. Analysis of alphaSMA-labeled progenitor cell commitment identifies Notch signaling as an important pathway in fracture healing. J Bone Miner Res. 2014;29(5):1283-94.
22. Grcevic D, Pejda S, Matthews BG, Repic D, Wang LP, Li HT, et al. In vivo fate mapping identifies mesenchymal progenitor cells. Stem Cells. 2012;30(2):187-96.
23. Arthur A, Nguyen TM, Paton S, Zannettino ACW, Gronthos S. Loss of EfnB1 in the osteogenic lineage compromises their capacity to support hematopoietic stem/progenitor cell maintenance. Exp Hematol. 2019;69:43-53.
24. Lundberg P, Allison SJ, Lee NJ, Baldock PA, Brouard N, Rost S, et al. Greater bone formation of Y2 knockout mice is associated with increased osteoprogenitor numbers and altered Y1 receptor expression. J Biol Chem. 2007;282(26):19082-91.
25. Kalajzic I, Kalajzic Z, Kaliterna M, Gronowicz G, Clark SH, Lichtler AC, et al. Use of type I collagen green fluorescent protein transgenes to identify subpopulations of cells at different stages of the osteoblast lineage. J Bone Miner Res. 2002;17(1):15-25.
26. Matic I, Matthews BG, Wang X, Dyment NA, Worthley DL, Rowe DW, et al. Quiescent bone lining cells are a major source of osteoblasts during adulthood. Stem Cells. 2016;34(12):2930-42.
27. Foudi A, Hochedlinger K, Van Buren D, Schindler JW, Jaenisch R, Carey V, et al. Analysis of histone 2B-GFP retention reveals slowly cycling hematopoietic stem cells. Nat Biotechnol. 2009;27(1):84-90.
28. Chakkalakal JV, Christensen J, Xiang W, Tierney MT, Boscolo FS, Sacco A, et al. Early forming label-retaining muscle stem cells require p27kip1 for maintenance of the primitive state. Development. 2014;141(8):1649-59.
29. Matthews BG, Wee NKY, Widjaja VN, Price JS, Kalajzic I, Windahl SH. alphaSMA Osteoprogenitor Cells Contribute to the Increase in Osteoblast Numbers in Response to Mechanical Loading. Calcif Tissue Int. 2020;106(2):208-17.
30. Mori Y, Adams D, Hagiwara Y, Yoshida R, Kamimura M, Itoi E, et al. Identification of a progenitor cell population destined to form fracture fibrocartilage callus in Dickkopf-related protein 3-green fluorescent protein reporter mice. J Bone Miner Metab. 2016;34(6):606-14.
31. Mashimo T, Saito T, Shiratsuchi H, Iwata J, Uryu T, Tamagawa T, et al. Assessment of the bone regenerative process from fibular periosteum by in vivo micro computed tomography. J Hard Tissue Biol. 2013;22(4):391-9.
32. Kuwahara ST, Serowoky MA, Vakhshori V, Tripuraneni N, Hegde NV, Lieberman JR, et al. Sox9+ messenger cells orchestrate large-scale skeletal regeneration in the mammalian rib. Elife. 2019;8.
33. Ozaki A, Tsunoda M, Kinoshita S, Saura R. Role of fracture hematoma and periosteum during fracture healing in rats: interaction of fracture hematoma and the periosteum in the initial step of the healing process. J Orthop Sci. 2000;5(1):64-70.
34. Zhang X, Xie C, Lin AS, Ito H, Awad H, Lieberman JR, et al. Periosteal progenitor cell fate in segmental cortical bone graft transplantations: implications for functional tissue engineering. J Bone Miner Res. 2005;20(12):2124-37.
35. Van Gastel N, Stegen S, Stockmans I, Moermans K, Schrooten J, Graf D, et al. Expansion of murine periosteal progenitor cells with fibroblast growth factor 2 reveals an intrinsic endochondral ossification program mediated by bone morphogenetic protein 2. Stem Cells. 2014;32(9):2407-18.
36. Wang X, Matthews BG, Yu J, Novak S, Grcevic D, Sanjay A, et al. PDGF modulates BMP2-induced osteogenesis in periosteal progenitor cells. JBMR Plus. 2019;3(5):e10127.
37. Chan CKF, Chen C-C, Luppen CA, Kim J-B, DeBoer AT, Wei K, et al. Endochondral ossification is required for haematopoietic stem-cell niche formation. Nature. 2009;457(7228):490-4.
38. Cherry HM, Roelofs AJ, Kurth TB, De Bari C. In vivo phenotypic characterisation of nucleoside label-retaining cells in mouse periosteum. Eur Cell Mater. 2014;27:185-95; discussion 95.

39. Wang L, Tower RJ, Chandra A, Yao L, Tong W, Xiong Z, et al. Periosteal mesenchymal progenitor dysfunction and extraskeletally-derived fibrosis contribute to atrophic fracture nonunion. J Bone Miner Res. 2019;34(3):520-32.
40. Abou-Khalil R, Yang F, Lieu S, Julien A, Perry J, Pereira C, et al. Role of muscle stem cells during skeletal regeneration. Stem Cells. 2015;33(5):1501-11.
41. Liu R, Birke O, Morse A, Peacock L, Mikulec K, Little DG, et al. Myogenic progenitors contribute to open but not closed fracture repair. BMC Musculoskelet Disord. 2011;12:288.
42. Kolind M, Bobyn JD, Matthews BG, Mikulec K, Aiken A, Little DG, et al. Lineage tracking of mesenchymal and endothelial progenitors in BMP-induced bone formation. Bone. 2015;81:53-9.
43. Matthews BG, Torreggiani E, Roeder E, Matic I, Grcevic D, Kalajzic I. Osteogenic potential of alpha smooth muscle actin expressing muscle resident progenitor cells. Bone. 2016;84:69-77.
44. Matsushita Y, Nagata M, Kozloff KM, Welch JD, Mizuhashi K, Tokavanich N, et al. A Wnt-mediated transformation of the bone marrow stromal cell identity orchestrates skeletal regeneration. Nat Commun. 2020;11(1).
45. He X, Bougioukli S, Ortega B, Arevalo E, Lieberman JR, McMahon AP. Sox9 positive periosteal cells in fracture repair of the adult mammalian long bone. Bone. 2017;103:12-9.
46. Kawanami A, Matsushita T, Chan YY, Murakami S. Mice expressing GFP and CreER in osteochondro progenitor cells in the periosteum. Biochem Biophys Res Commun. 2009;386(3):477-82.
47. Kalajzic Z, Li H, Wang LP, Jiang X, Lamothe K, Adams DJ, et al. Use of an alpha-smooth muscle actin GFP reporter to identify an osteoprogenitor population. Bone. 2008;43(3):501-10.
48. Dyment NA, Hagiwara Y, Matthews BG, Li Y, Kalajzic I, Rowe DW. Lineage tracing of resident tendon progenitor cells during growth and natural healing. PLoS ONE. 2014;9(4):e96113.
49. Roguljic H, Matthews BG, Yang W, Cvija H, Mina M, Kalajzic I. In vivo Identification of periodontal progenitor cells. J Dent Res. 2013;92(8):709-15.
50. Vidovic I, Banerjee A, Fatahi R, Matthews BG, Dyment NA, Kalajzic I, et al. alphaSMA-expressing perivascular cells represent dental pulp progenitors in vivo. J Dent Res. 2017;96(3):323-30.
51. Zhao H, Feng JF, Ho TV, Grimes W, Urata M, Chai Y. The suture provides a niche for mesenchymal stem cells of craniofacial bones. Nat Cell Biol. 2015;17(4):386-+.
52. Maruyama T, Jeong J, Sheu TJ, Hsu W. Stem cells of the suture mesenchyme in craniofacial bone development, repair and regeneration. Nat Commun. 2016;7.
53. Wilk K, Yeh SCA, Mortensen LJ, Ghaffarigarakani S, Lombardo CM, Bassir SH, et al. Postnatal calvarial skeletal stem cells expressing PRX1 reside exclusively in the calvarial sutures and are required for bone regeneration. Stem Cell Rep. 2017;8(4):933-46.
54. Madisen L, Zwingman TA, Sunkin SM, Oh SW, Zariwala HA, Gu H, et al. A robust and high-throughput Cre reporting and characterization system for the whole mouse brain. Nat Neurosci. 2010;13(1):133-40.
55. Voehringer D, Liang HE, Locksley RM. Homeostasis and effector function of lymphopenia-induced "memory-like" T cells in constitutively T cell-depleted mice. J Immunol. 2008;180(7):4742-53.
56. Kim JE, Nakashima K, de Crombrugghe B. Transgenic mice expressing a ligand-inducible cre recombinase in osteoblasts and odontoblasts: a new tool to examine physiology and disease of postnatal bone and tooth. Am J Pathol. 2004;165(6):1875-82.
57. Matthews BG, Roeder E, Wang X, Aguila HL, Lee SK, Grcevic D, et al. Splenomegaly, myeloid lineage expansion and increased osteoclastogenesis in osteogenesis imperfecta murine. Bone. 2017;103:1-11.
58. Dyment NA, Jiang X, Chen L, Hong SH, Adams DJ, Ackert-Bicknell C, et al. High-throughput, multi-image cryohistology of mineralized tissues. J Vis Exp. 2016;115:e54468.
59. Novak S, Roeder E, Sinder BP, Adams DJ, Siebel CW, Grcevic D, et al. Modulation of Notch1 signaling regulates bone fracture healing. J Orthop Res. 2020.

Figure legends

Figure 1: Mesenchymal stem cell markers are enriched in periosteum

Flow cytometry and cell sorting was used to evaluate marker expression in tissue from adult long bones. (A) Expression of markers in periosteum, endosteum and bone marrow samples as a percentage of the CD45/Ter119/CD31- fraction, n=4-46. Expression in periosteum is significantly different from both bone marrow and endosteum for all markers (2-way ANOVA with post test comparing cell types). (B) CFU-F formation in the total CD45/Ter119/CD31- fraction. (C) Marker expression on Col2.3GFP+ osteoblasts, n=4-24. (D) Gating to identify bone, cartilage and stromal progenitors (BCSP) and skeletal stem cells (SSC), and presence of endosteal Col2.3GFP+ osteoblasts as a major component of these populations (mean±SD, n=22). (E) Frequency of BCSP and SSC populations in different tissue compartments and populations (n=8, bone marrow; n=22, other samples). (F) CFU-F of different periosteal populations (n=3). * $p<0.05$ compared to total CD45- based on 1-way ANOVA with Dunnett's post test. (G) Differentiation potential of cell populations grown in mixed osteogenic adipogenic conditions. Pink is ALP stain, red is oil red O, colonies indicated show ostegenic only (blue arrowhead), adipogenic only (black arrowhead) and mixed (*) colonies. ND, not determined.

Figure 2: Label-retaining cells are enriched for most progenitor markers

(A) Experimental design for label-retaining cell experiments. (B) Femoral cortical histology showing H2B-GFP expression following 5 weeks dox. Periosteum (p) and bone marrow (bm) are indicated. (C) Femoral cortical histology following 13 weeks chase. LRCs in the periosteum are indicated by arrowheads. GFP signal is enhanced compared to B. (D) Representative gating of the CD45- population in different periosteum samples to define three populations based on GFP expression. (E) Quantification of different GFP populations in a representative experiment for periosteum and endosteum (n=1, no dox; n=4, no chase; n=6, 13w chase). (F) CFU-F frequency in different GFP populations in no chase samples (n=3), and (G) following chase (n=6). Cell surface marker expression

is shown in different CD45- GFP subsets following chase in (H) periosteum cells and (I) endosteal cells. Data is pooled from 3 separate experiments involving 13-22 weeks chase (n=19). * $p<0.05$, repeated measures ANOVA with Dunnett's post test compared to GFP- population. Scale bars are 100µm.

Figure 3: αSMA identifies long term progenitor cells in the periosteum

Representative images of tibia mid-shaft periosteum (A) 14 days or (B) 56 days after tamoxifen with the periosteal surface near the top and endosteal surface near the bottom of the image. Percentage of αSMA-labeled (Tom+) cells within the CD45- population at different time points in (C) periosteum and (D) endosteum as measured by flow cytometry (n=2-5). Fracture histology of representative day 7 tibial fracture calluses in different groups: (E) αSMA-labeled with tamoxifen at day -1, 0; (F) αSMA-labeled with tamoxifen at day -91, -90; (G) Col2.3-labeled with tamoxifen at day -4, -3. Quantification of αSMA-labeled cell contribution to Col2.3GFP+ osteoblasts in the fracture callus based on image analysis in (H) day 7 fracture callus and (I) day 14 fracture callus at different times after tamoxifen administration. (J) Quantification of αSMA-labeled cell contribution to Sox9+ chondrocytes in day 7 fracture callus. (K) Quantification of Col2.3-labeled cell contribution to Osx+ osteoblasts. All images show mineralized bone by dark field (gray), and DAPI+ nuclei in blue. Scale bars are 100µm (A,B) or 250µm (E-G). In F, the boxed area is magnified and αSMA-labeled osteoblasts as quantified in H-I are indicated with arrowheads. Approximate callus area used for analysis is indicated by the dashed lines in E-G, cortical bone surface defines the inner boundary. * $p<0.05$ compared to no tamoxifen control with ANOVA followed by Dunnett's post test. # $p<0.05$ compared to tamoxifen day 0 group.

Figure 4: Further characterization of αSMA-labeled cells

(A) Representative flow plot showing gating of αSMA-labeled cells. (B) Proportion of αSMA-labeled cells 2-3 days after tamoxifen in different tissue compartments (n=17). Cell surface marker expression in the Tomato+ population 2-3 days after tamoxifen in (C) periosteum and (D) endosteum

(n=4-17). (E) Cell surface profile of αSMA-labeled cells at different time points. (F) CFU-F frequency of αSMA-labeled cells sorted 2 days after tamoxifen. (G) Engraftment of transplanted αSMA-labeled cells in a calvarial defect 5 weeks after transplantation. Arrowheads indicate cells that are Col2.3GFP+. (H) Representative plots showing identification of αSMA-labeled label-retaining cells. Values represent an average of n=3-10. (I) CFU-F formation and (J) differentiation of colonies under mixed osteogenic/adipogenic conditions of αSMA-labeled label-retaining cells and other subpopulations (n=5 for CFU-F, n=3 for differentiation). (K) Cell-surface marker expression in αSMA-labeled subpopulations. * $p<0.05$ compared to black bars, # $p<0.05$ compared to Tom+GFP- population. Scale bars indicate 200µm (low magnification) and 100µm (high magnification).

Figure 5: Ablation of αSMA+ cells impairs fracture healing.

(A) Flow cytometry of day 4 fracture callus from control αSMACreER/Ai9 mice and DTA animals (αSMACreER/Rosa-DTA/Ai9) indicating significantly fewer ($p<0.01$) labeled cells in the ablation model (mean±SD shown), n=4. (B) Representative histological sections from day 4 fracture callus in controls or with DTA-mediated ablation. The outline of the callus is indicated. (C-D) MicroCT analysis of day 14 fracture callus in control mice or those that had undergone two different tamoxifen regimens to ablate αSMA+ cells, day 0, 1 of fracture or day 0, 2, 4, 6, 8. Callus tissue volume (C) and bone mass (D) were measured. Cre- n=14, 8 male 6 female; DTA D0-1 n=10, 4M 6F; DTA D0-8 n=8 4M 4F).

Figure S1 (related to Figure 1): Flow cytometry plots of mesenchymal progenitor marker expression

Representative plots showing (A) the initial gating scheme to enable analysis of mesenchymal cell populations, and expression of indicated markers CD45/CD31/Ter119- cells in (B) periosteum, (C) endosteum and (D) bone marrow of representative samples in relation to Sca1. Quadrant percentages are specific to the sample that is shown. The periosteum, endosteum and bone marrow samples in each column come from the same sample (obtained from 2 animals). FSC, forward scatter; SSC, side scatter.

Figure S2 (related to Figure 2): Histology of H2B-GFP/αSMACreER/Ai9 femurs

(A) H2B-GFP expression in a distal femur following 5 weeks dox, and 2 days after tamoxifen. (B) H2B-GFP label-retaining cells after 13 weeks chase, tamoxifen was given at the time of dox withdrawal. Boxed areas are magnified. The same bones shown in Figure 2B and C are presented here with Tomato expression shown; gp, growth plate. Scale bars are 250µm or 100µm (high magnification images).

Figure S3 (related to Figure 3): αSMA lineage tracing in the bone marrow compartment of juvenile mice.

Lineage tracing in the distal femur of αSMACreER/Ai9 mice at different time points after tamoxifen treatment at 4-5 weeks of age. (A) and (B) are replicates of data shown in Grcevic et al (22). Both show background signal in bone marrow in green, and (C-F) have DAPI staining in blue. After 17 days, many osteoblasts and osteocytes in trabeculae are labeled, but at day 70 magnified areas show few labeled cells are present in the primary spongiosa (D), but labeled osteocytes are retained in more proximal trabeculae (E) and in some cortical regions (F). Muscle is labeled due to targeting of some satellite cells by αSMACreER (43). Scale bars are 250µm (A-C) and 100µm (D-F). gp, growth plate.

Figure S4 (related to Figure 3): αSMA lineage tracing in the bone marrow compartment of adult mice.

Proximal tibia trabecular histology in αSMACreER/Ai9/Col2.3GFP mice 14 days (A) and 100 days (B) after tamoxifen treatment during adulthood (at least 8 weeks of age). Note that there are few red cells, and almost no contribution to osteoblasts or osteocytes. Scale bars are 250µm. gp, growth plate.

Figure S5 (related to Figure 3): Minimal αSMACreER leakiness in fracture callus, and contribution to endosteal bone formation.

(A) Fracture histology of representative day 7 callus in an αSMACreER/Ai9/Col2.3GFP mouse never exposed to tamoxifen showing the red channel only and merged image. The magnified images show the boxed area. A small number of red cells are visible, however very few colocalize with Col2.3GFP. Callus area is outlined in white. Scale bar is 250µm. (B) Contribution of αSMA-labeled cells to new Col2.3GFP+ osteoblasts in the bone marrow compartment (as indicated by pink box in A) in day 7 fractures, and (C) in day 14 fractures. * $p<0.05$ compared to no tamoxifen control with ANOVA followed by Dunnett's post test. # $p<0.05$ compared to tamoxifen day 0 group using similar ANOVA.

Figure 1

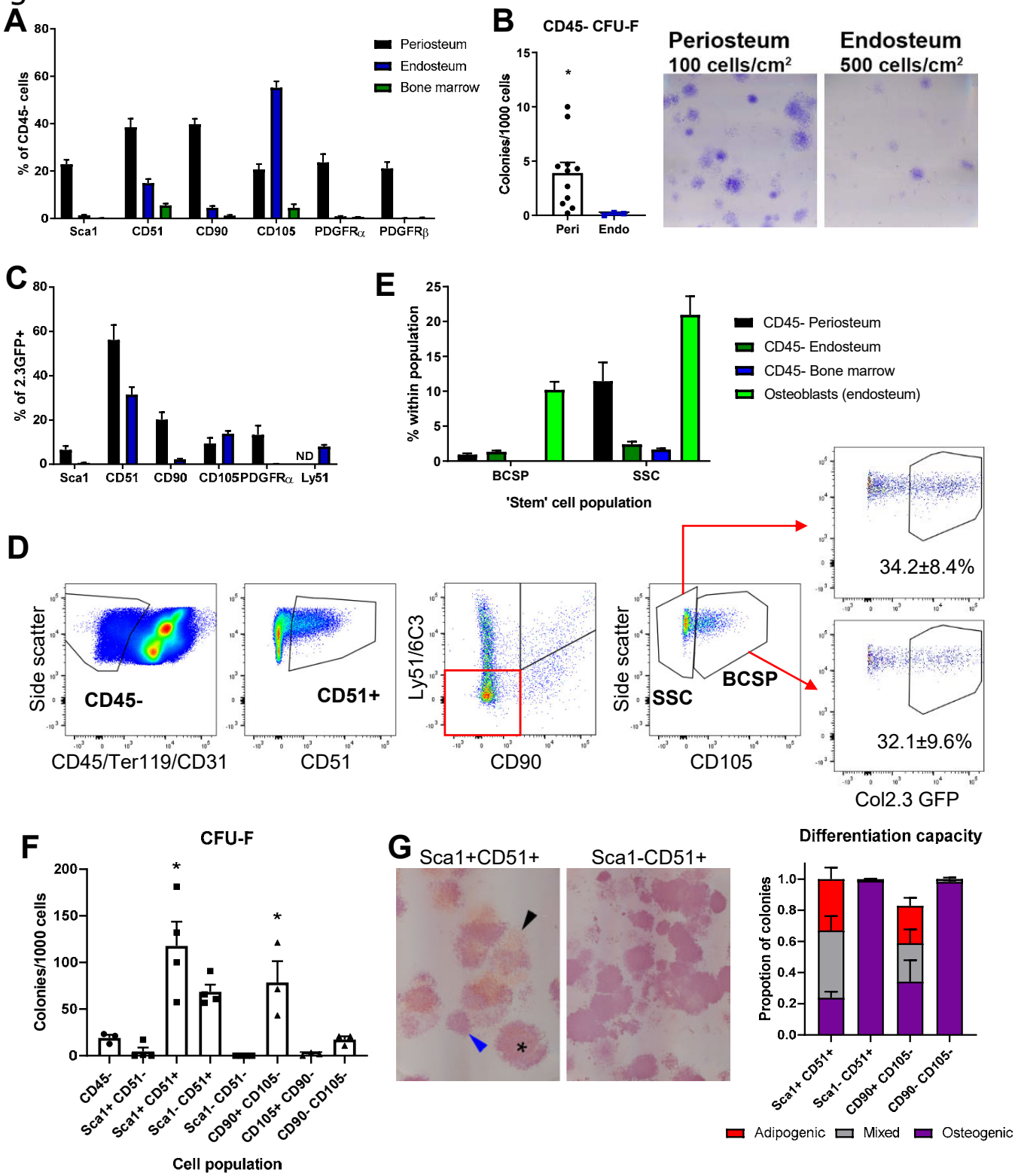

Figure 1: Mesenchymal stem cell markers are enriched in periosteum

Flow cytometry and cell sorting was used to evaluate marker expression in tissue from adult long bones. (A) Expression of markers in periosteum, endosteum and bone marrow samples as a percentage of the CD45/Ter119/CD31- fraction, n=4-46 (see Table S2). Expression in periosteum is significantly different from both bone marrow and endosteum for all markers (2-way ANOVA with post test comparing cell types). (B) CFU-F formation in the total CD45/Ter119/CD31- fraction. (C) Marker expression on Col2.3GFP+ osteoblasts, n=4-24. (D) Gating to identify bone, cartilage and stromal progenitors (BCSP) and skeletal stem cells (SSC), and presence of endosteal Col2.3GFP+ osteoblasts as a major component of these populations (mean±SD, n=22). (E) Frequency of BCSP and SSC populations in different tissue compartments and populations (n=8, bone marrow; n=22, other samples). (F) CFU-F of different periosteal populations (n=3). * $p<0.05$ compared to total CD45- based on 1-way ANOVA with Dunnett's post test. (G) Differentiation potential of cell populations grown in mixed osteogenic adipogenic conditions. Pink is ALP stain, red is oil red O, colonies indicated show ostegenic only (blue arrowhead), adipogenic only (black arrowhead) and mixed (*) colonies. ND, not determined.

Figure 2

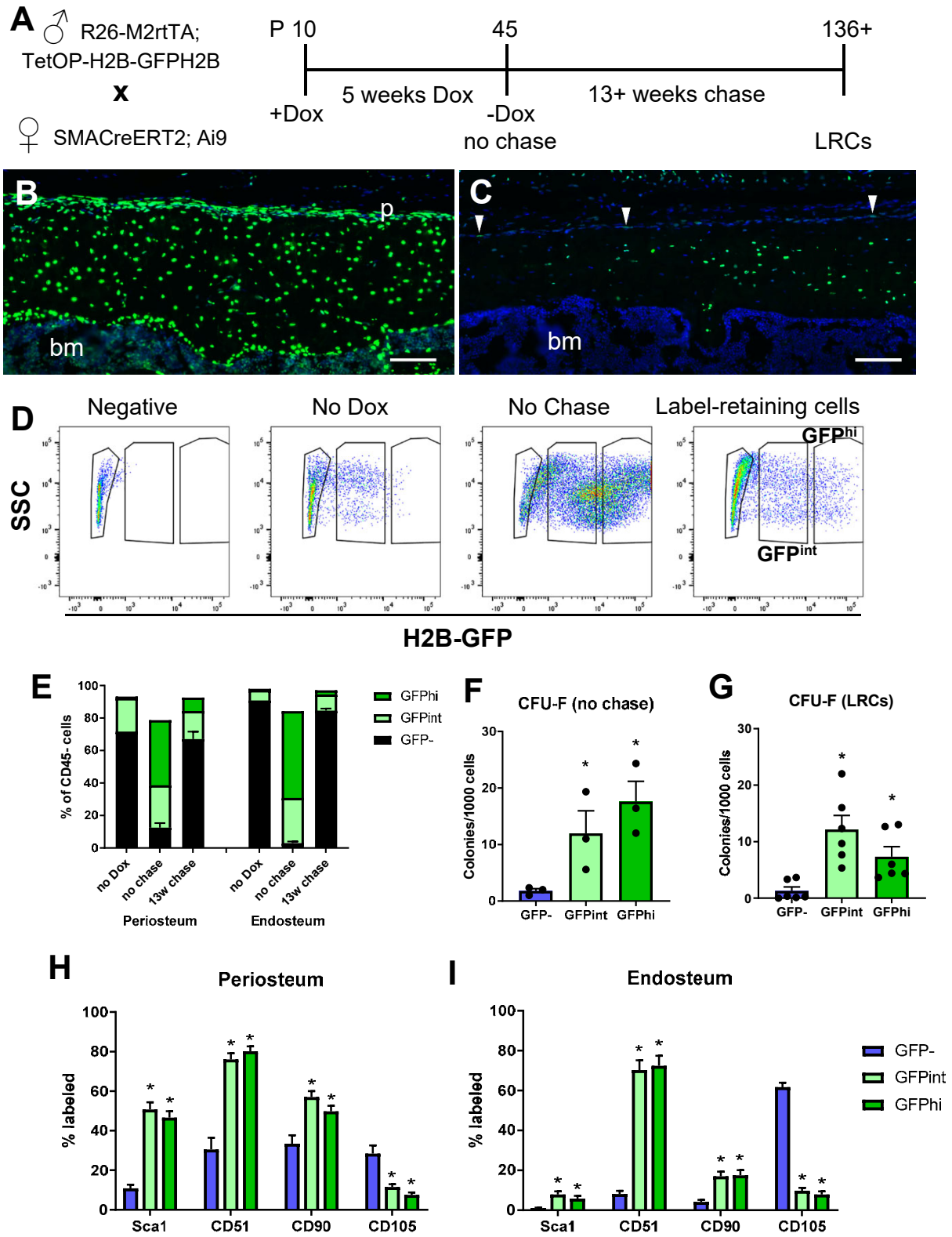

Figure 2: Label-retaining cells are enriched for most progenitor markers
(A) Experimental design for label-retaining cell experiments. (B) Femoral cortical histology showing H2B-GFP expression following 5 weeks dox. Periosteum (p) and bone marrow (bm) are indicated. (C) Femoral cortical histology following 13 weeks chase. LRCs in the periosteum are indicated by arrowheads. GFP signal is enhanced compared to B. (D) Representative gating of the CD45- population in different periosteum samples to define three populations based on GFP expression. (E) Quantification of different GFP populations in a representative experiment for periosteum and endosteum (n=1, no dox; n=4, no chase; n=6, 13w chase). (F) CFU-F frequency in different GFP populations in no chase samples (n=3), and (G) following chase (n=6). Cell surface marker expression is shown in different CD45- GFP subsets following chase in (H) periosteum cells and (I) endosteal cells. Data is pooled from 3 separate experiments involving 13-22 weeks chase (n=19). * $p<0.05$, repeated measures ANOVA with Dunnett's post test compared to GFP- population. Scale bars are 100µm.

Figure 3

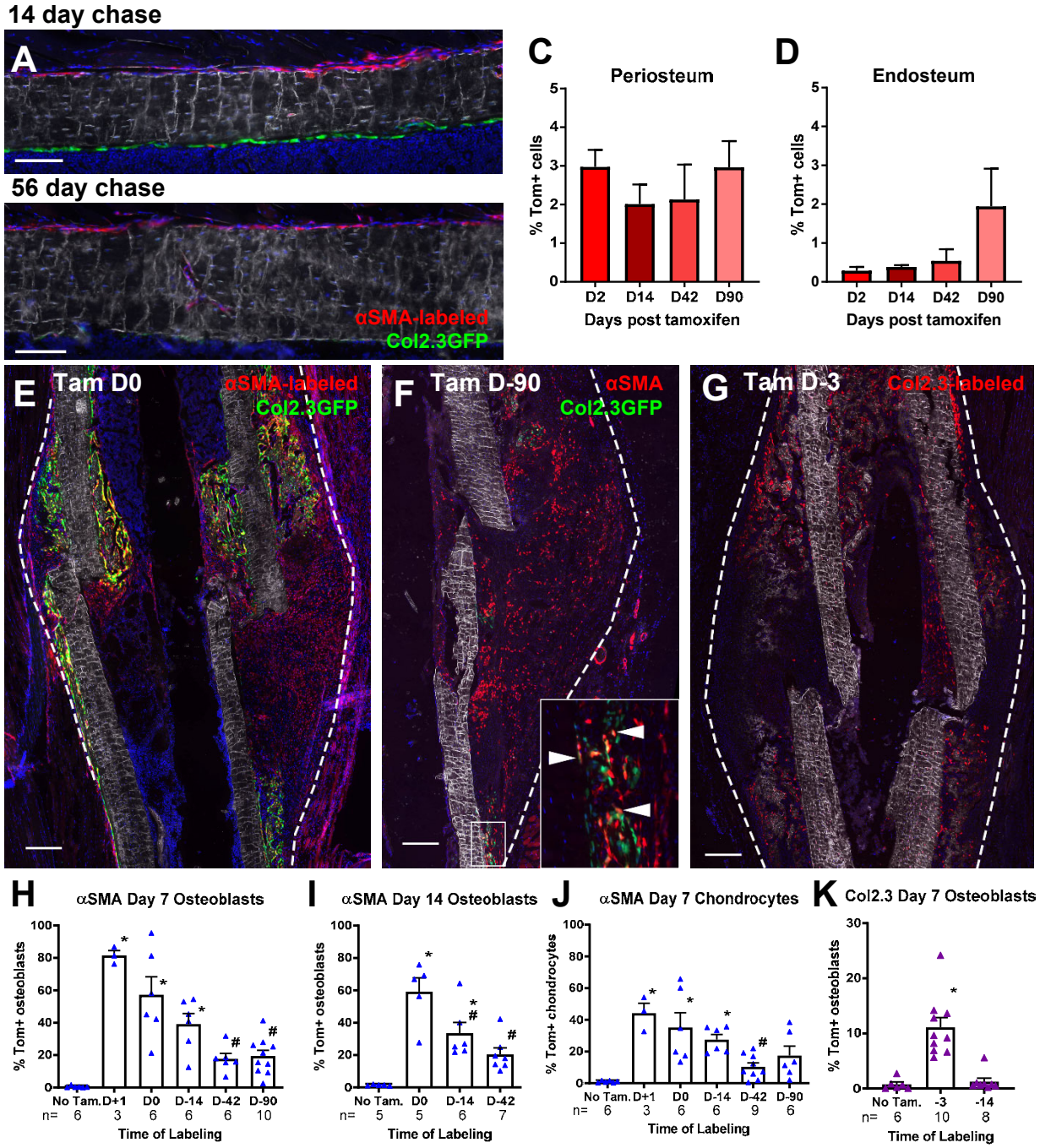

Figure 3: αSMA identifies long term progenitor cells in the periosteum
Representative images of tibia mid-shaft periosteum (A) 14 days or (B) 56 days after tamoxifen with the periosteal surface near the top and endosteal surface near the bottom of the image. Percentage of αSMA-labeled (Tom+) cells within the CD45- population at different time points in (C) periosteum and (D) endosteum as measured by flow cytometry (n=2-5). Fracture histology of representative day 7 tibial fracture calluses in different groups: (E) αSMA-labeled with tamoxifen at day -1, 0; (F) αSMA-labeled with tamoxifen at day -91, -90; (G) Col2.3-labeled with tamoxifen at day -4, -3. Quantification of αSMA-labeled cell contribution to Col2.3GFP+ osteoblasts in the fracture callus based on image analysis in (H) day 7 fracture callus and (I) day 14 fracture callus at different times after tamoxifen administration. (J) Quantification of αSMA-labeled cell contribution to Sox9+ chondrocytes in day 7 fracture callus. (K) Quantification of Col2.3-labeled cell contribution to Osx+ osteoblasts. All images show mineralized bone by dark field (gray), and DAPI+ nuclei in blue. Scale bars are 100µm (A,B) or 250µm (E-G). In F, the boxed area is magnified and αSMA-labeled osteoblasts as quantified in H-I are indicated with arrowheads. Approximate callus area used for analysis is indicated by the dashed lines in E-G, cortical bone surface defines the inner boundary. * $p<0.05$ compared to no tamoxifen control with ANOVA followed by Dunnett's post test. # $p<0.05$ compared to tamoxifen day 0 group.

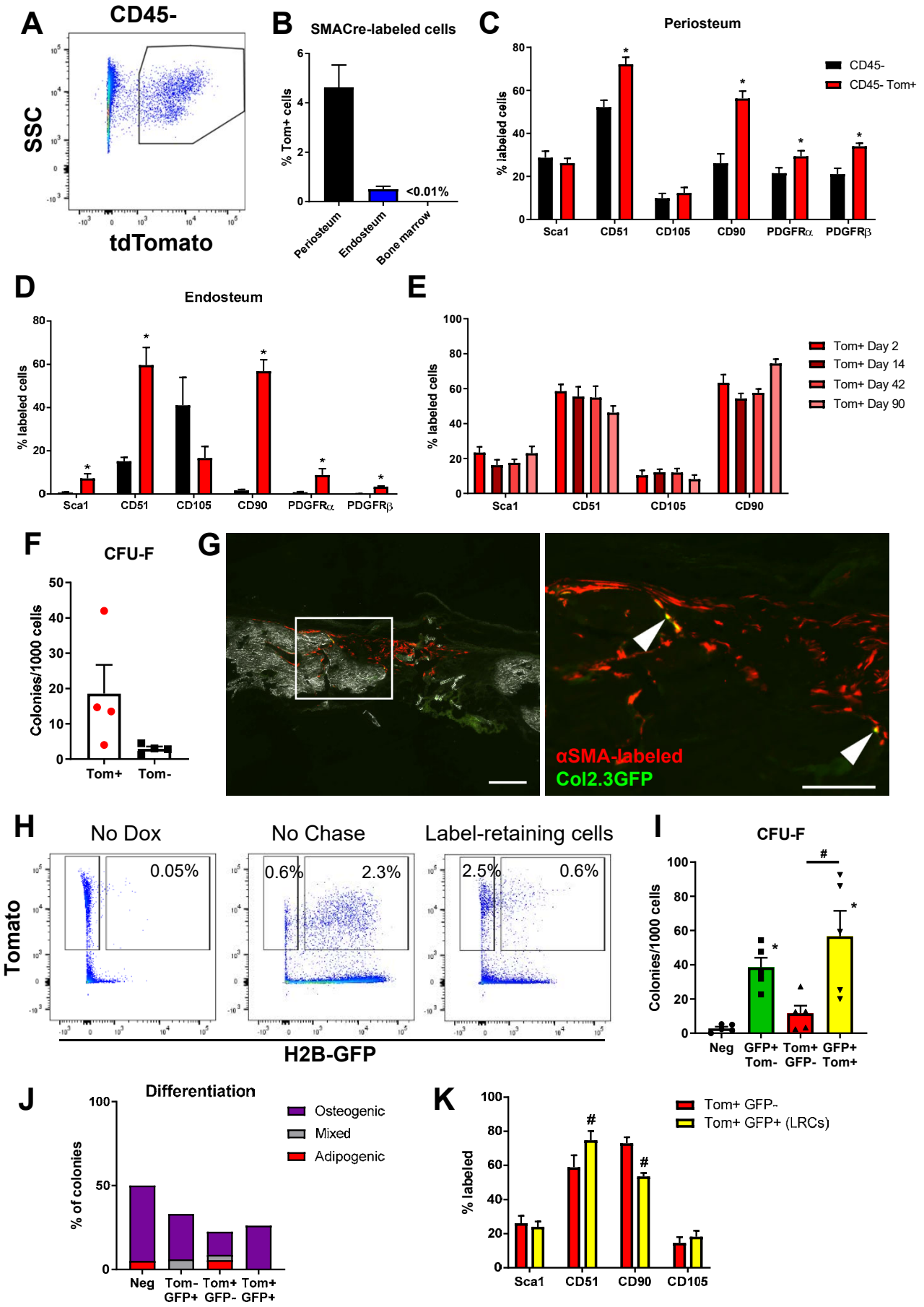

Figure 4: Further characterization of αSMA-labeled cells

(A) Representative flow plot showing gating of αSMA-labeled cells. (B) Proportion of αSMA-labeled cells 2-3 days after tamoxifen in different tissue compartments (n=17). Cell surface marker expression in the Tomato+ population 2-3 days after tamoxifen in (C) periosteum and (D) endosteum (n=4-17, see Table S2). (E) Cell surface profile of αSMA-labeled cells at different time points. (F) CFU-F frequency of αSMA-labeled cells sorted 2 days after tamoxifen. (G) Engraftment of transplanted αSMA-labeled cells in a calvarial defect 5 weeks after transplantation. Arrowheads indicate cells that are Col2.3GFP+. (H) Representative plots showing identification of αSMA-labeled label-retaining cells. Values represent an average of n=3-10. (I) CFU-F formation and (J)

Figure 4: Further characterization of αSMA-labeled cells

(A) Representative flow plot showing gating of αSMA-labeled cells. (B) Proportion of αSMA-labeled cells 2-3 days after tamoxifen in different tissue compartments (n=17). Cell surface marker expression in the Tomato+ population 2-3 days after tamoxifen in (C) periosteum and (D) endosteum (n=4-17, see Table S2). (E) Cell surface profile of αSMA-labeled cells at different time points. (F) CFU-F frequency of αSMA-labeled cells sorted 2 days after tamoxifen. (G) Engraftment of transplanted αSMA-labeled cells in a calvarial defect 5 weeks after transplantation. Arrowheads indicate cells that are Col2.3GFP+. (H) Representative plots showing identification of αSMA-labeled label-retaining cells. Values represent an average of n=3-10. (I) CFU-F formation and (J) differentiation of colonies under mixed osteogenic/adipogenic conditions of αSMA-labeled label-retaining cells and other subpopulations (n=5 for CFU-F, n=3 for differentiation). (K) Cell-surface marker expression in αSMA-labeled subpopulations. * $p<0.05$ compared to black bars, # $p<0.05$ compared to Tom+GFP- population. Scale bars indicate 200µm (low magnification) and 100µm (high magnification).

Figure 5

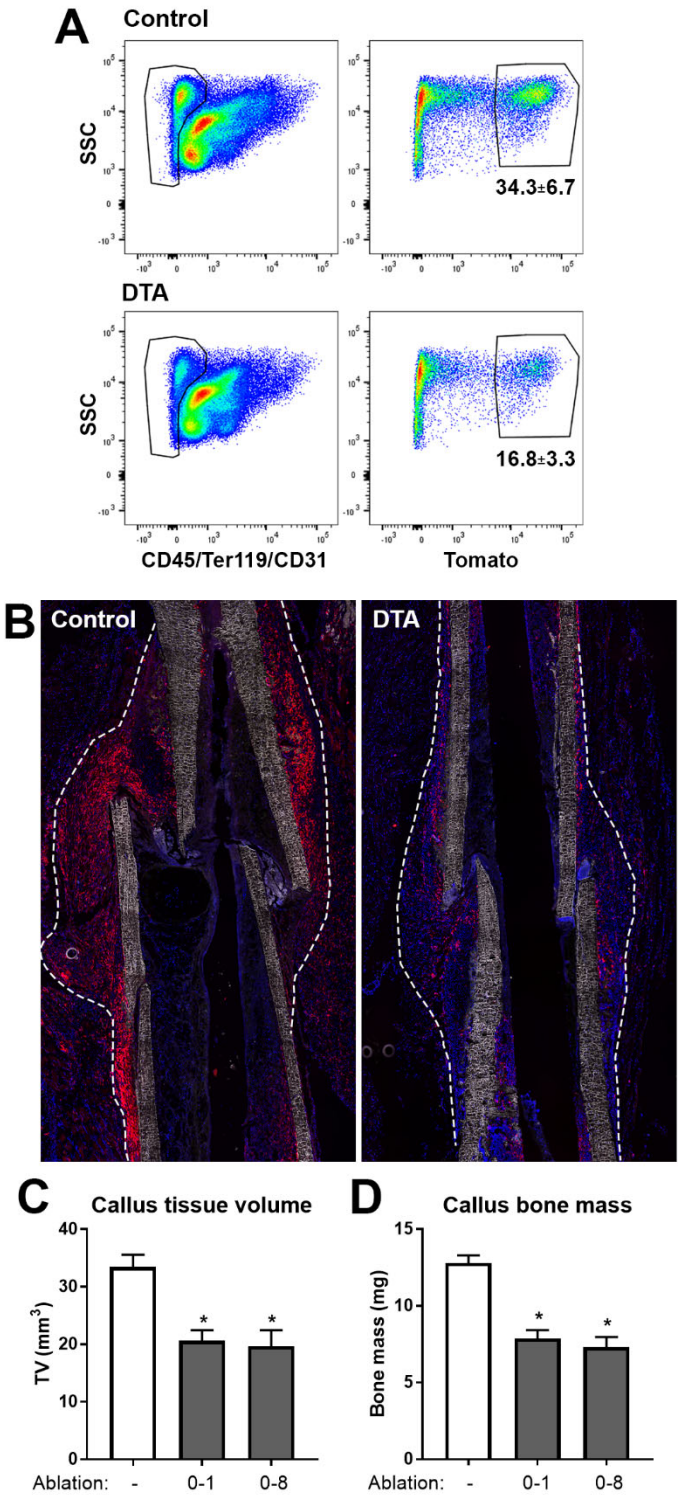

Figure 5: Ablation of αSMA+ cells impairs fracture healing.
(A) Flow cytometry of day 4 fracture callus from control αSMACreER/Ai9 mice and DTA animals (αSMACreER/Rosa-DTA/Ai9) indicating significantly fewer ($p<0.01$) labeled cells in the ablation model (mean±SD shown), n=4. (B) Representative histological sections from day 4 fracture callus in controls or with DTA-mediated ablation. The outline of the callus is indicated. (C-D) MicroCT analysis of day 14 fracture callus in control mice or those that had undergone two different tamoxifen regimens to ablate αSMA+ cells, day 0, 1 of fracture or day 0, 2, 4, 6, 8. Callus tissue volume (C) and bone mass (D) were measured. Cre- n=14, 8 male 6 female; DTA D0-1 n=10, 4M 6F; DTA D0-8 n=8 4M 4F).

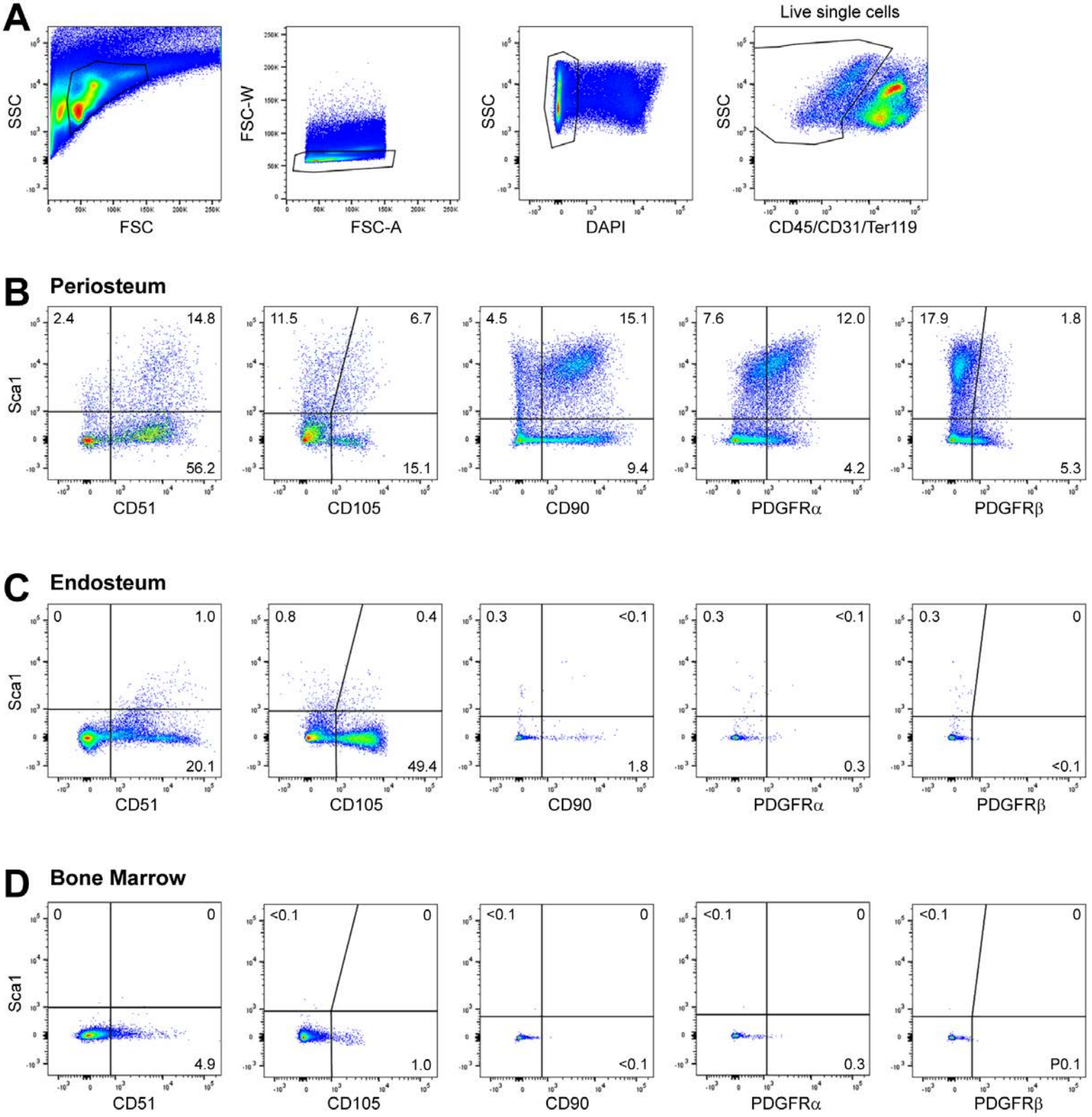
A
Live single cells
SSC
FSC
FSC-W
FSC-A
SSC
DAPI
SSC
CD45/CD31/Ter119
B
Periosteum
Sca1
CD51
CD105
CD90
PDGFRα
PDGFRβ
2.4
14.8
56.2
11.5
6.7
15.1
4.5
15.1
9.4
7.6
12.0
4.2
17.9
1.8
5.3
C
Endosteum
Sca1
CD51
CD105
CD90
PDGFRα
PDGFRβ
0
1.0
20.1
0.8
0.4
49.4
0.3
<0.1
1.8
0.3
<0.1
0.3
0.3
0
<0.1
D
Bone Marrow
Sca1
CD51
CD105
CD90
PDGFRα
PDGFRβ
0
0
4.9
<0.1
0
1.0
<0.1
0
<0.1
<0.1
0
0.3
<0.1
0
P0.1

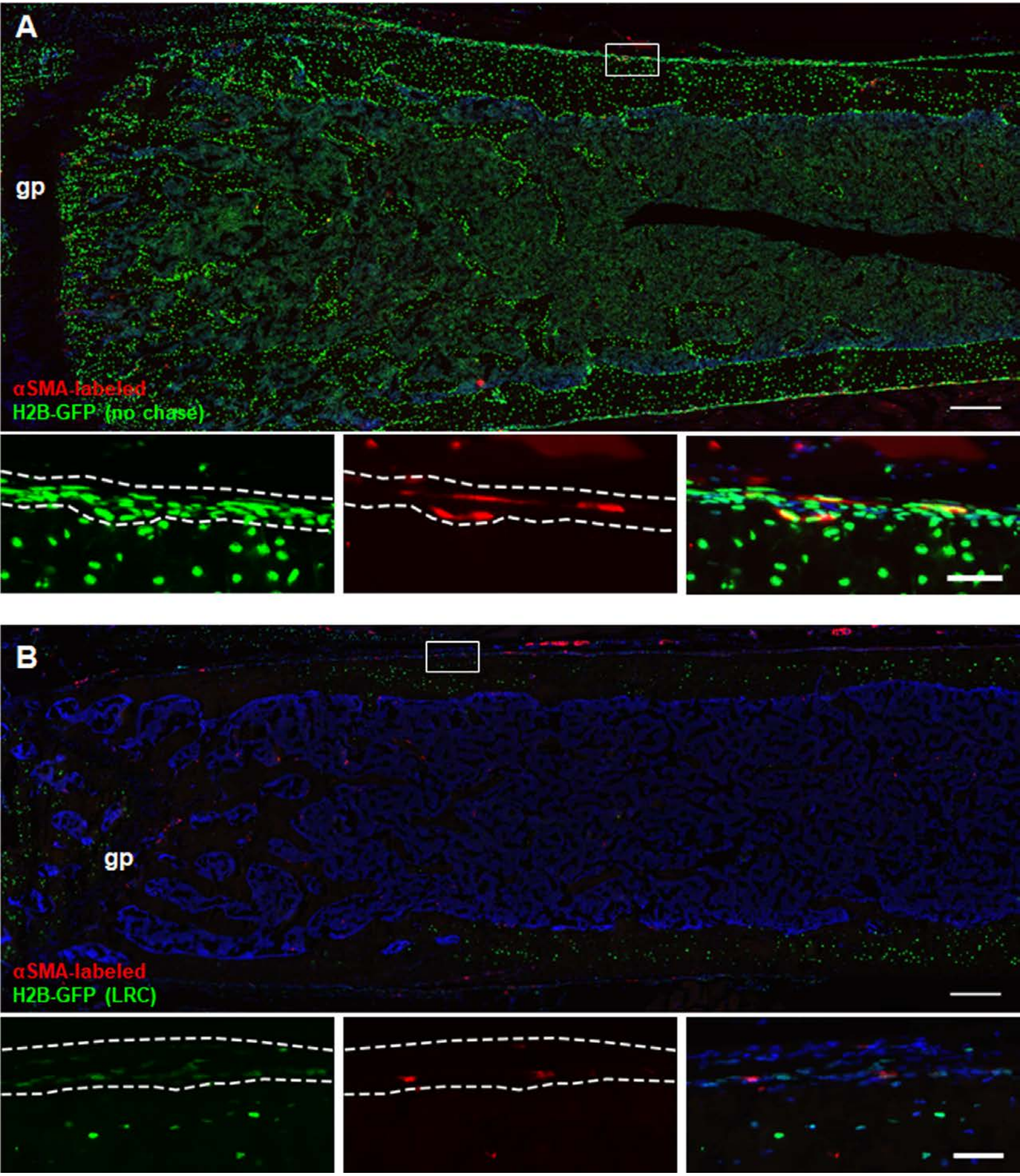
A
gp
αSMA-labeled
H2B-GFP (no chase)
B
gp
αSMA-labeled
H2B-GFP (LRC)

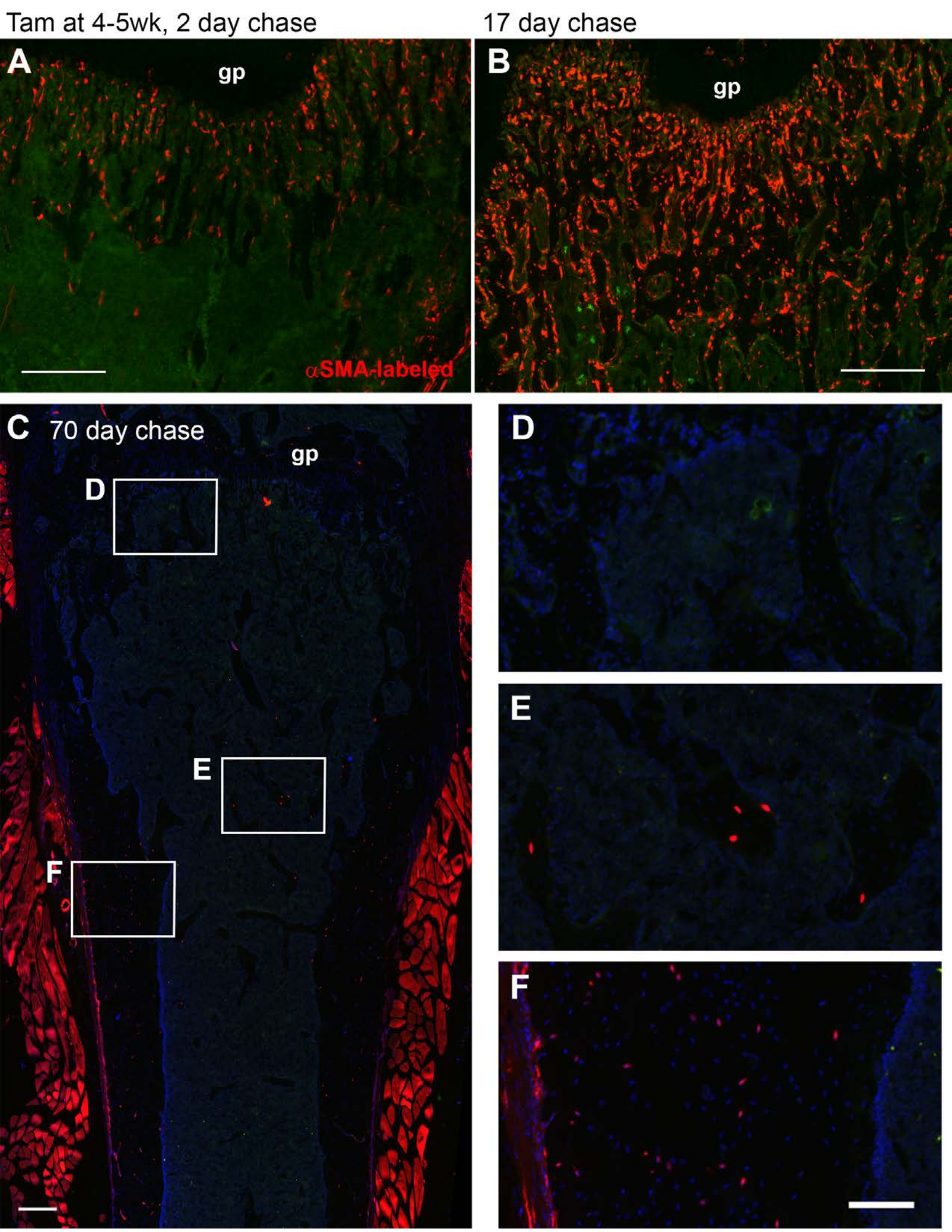
Tam at 4-5wk, 2 day chase
17 day chase
A
gp
αSMA-labeled
B
gp
C
70 day chase
gp
D
E
F
D
E
F

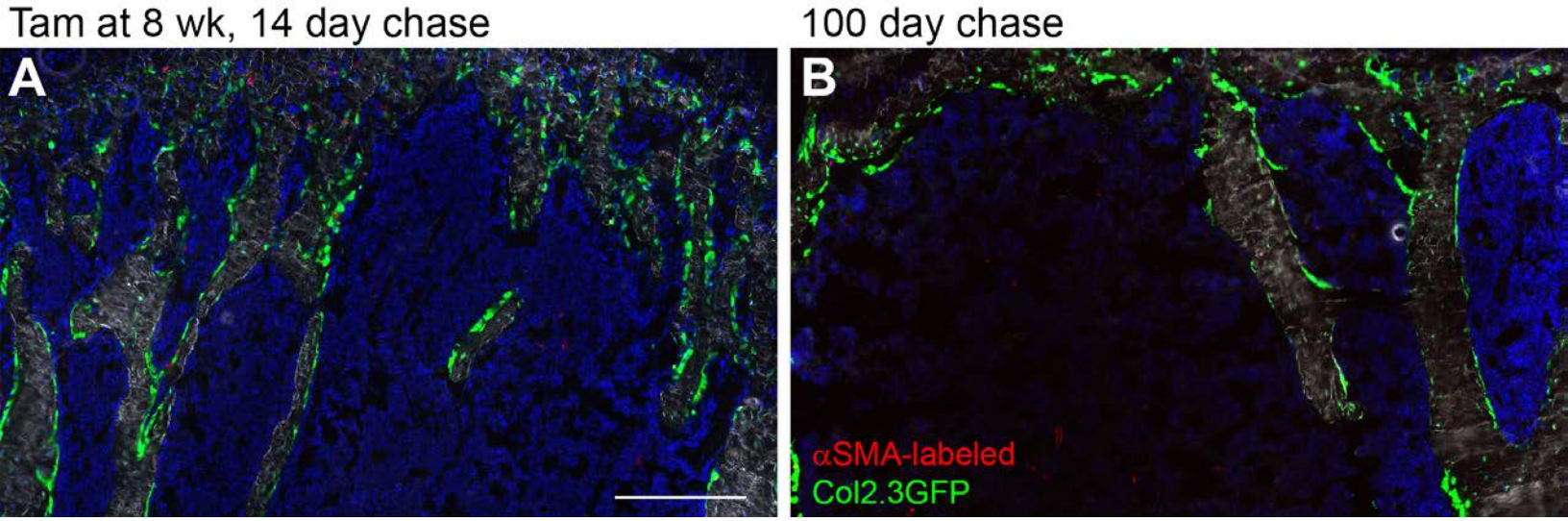
Tam at 8 wk, 14 day chase
100 day chase
A
B
αSMA-labeled
Col2.3GFP

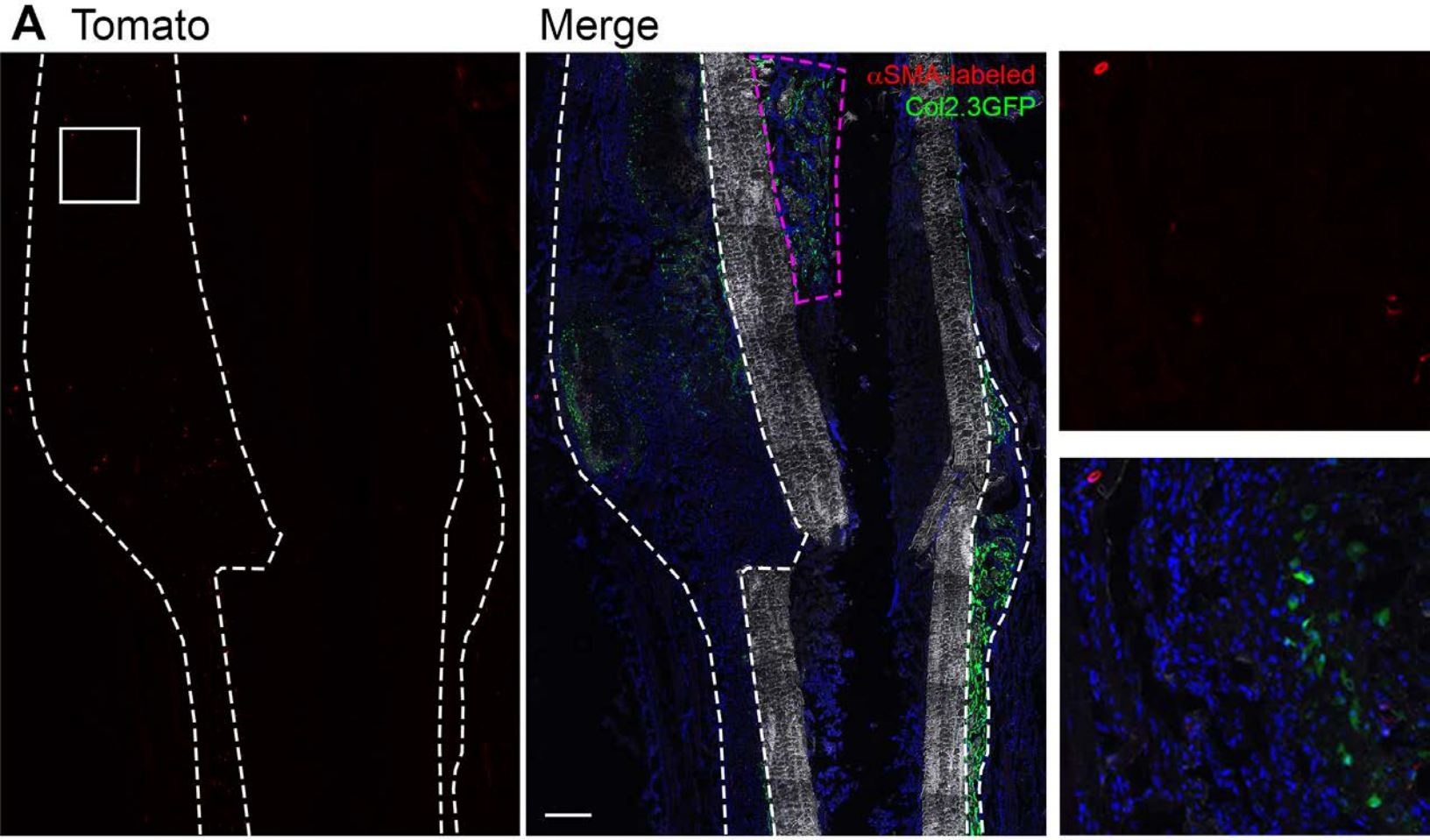
A
Tomato
Merge
αSMA-labeled
Col2.3GFP

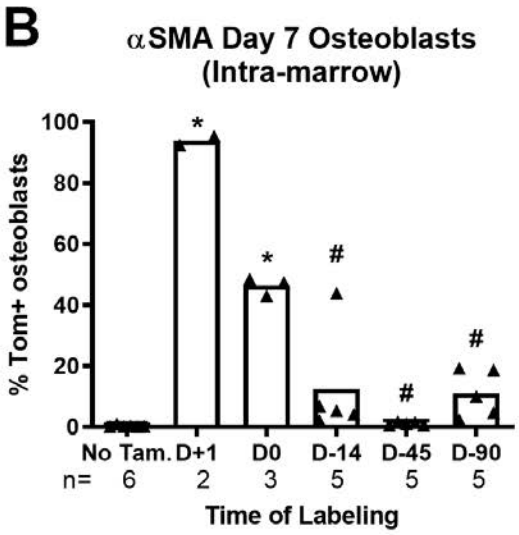
B
αSMA Day 7 Osteoblasts
(Intra-marrow)
% Tom+ osteoblasts
100
80
60
40
20
0
No Tam.
D+1
D0
D-14
D-45
D-90
n= 6 2 3 5 5 5
Time of Labeling

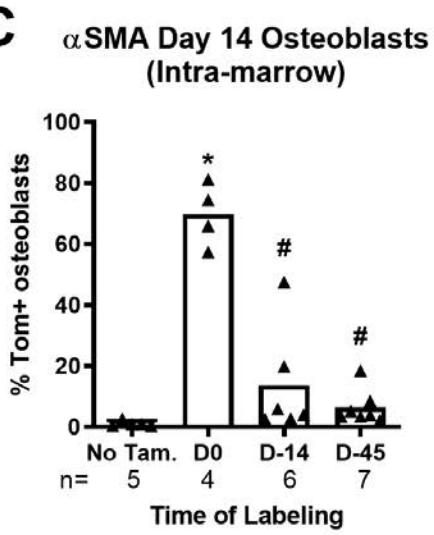
C
αSMA Day 14 Osteoblasts
(Intra-marrow)
% Tom+ osteoblasts
100
80
60
40
20
0
No Tam.
D0
D-14
D-45
n= 5 4 6 7
Time of Labeling